American Mineralogist, Volume 101, pages 1642–1650, 2016

Metastable structural transformations and pressure-induced amorphization in natural $(Mg,Fe)_2SiO_4$ olivine under static compression: A Raman spectroscopic study

David Santamaria-Perez[1,2], Andrew Thomson[1], Alfredo Segura[2], Julio Pellicer-Torres[2], Francisco J. Manjon[3], Furio Corà[4], Kit McColl[4], Mark Wilson[5], David Dobson[1], and Paul F. McMillan[4,*]

[1]Earth Sciences Department, University College London, Gower Street, London WC1E 6BT, U.K.
[2]Departamento de Física Aplicada-ICMUV, Universidad de València, 46010 València, Spain
[3]Instituto de Diseño para la Fabricación y Producción Automatizada, Universitat Politècnica de València, 46022 València, Spain
[4]Department of Chemistry, Christopher Ingold Laboratory, University College London, London WC1H 0AJ, U.K.
[5]Department of Chemistry, Physical and Theoretical Chemistry Laboratory, University of Oxford, South Parks Road, Oxford OX1 3QZ, U.K.

Abstract

Raman spectroscopic data were obtained for $(Mg,Fe)_2SiO_4$ samples during compression to 57 GPa. Single crystals of San Carlos olivine compressed hydrostatically above 41 GPa showed appearance of a new "defect" peak in the 820–840 cm^{-1} region associated with SiOSi linkages appearing between adjacent SiO_4^{4-} tetrahedra to result in five- or sixfold-coordinated silicate species. Appearance of this feature is accompanied by a broad amorphous background. The changes occur at lower pressure than metastable crystalline transitions of end-member Mg_2SiO_4 forsterite (Fo-I) into Fo-II and Fo-III phases described recently. We complemented our experimental study using density functional theory (DFT) calculations and anisotropic ion molecular dynamics (AIMD) simulations to study the Raman spectra and vibrational density of states (VDOS) of metastably compressed Mg_2SiO_4 olivine, Fo-II and Fo-III, and quenched melts at high and low pressures. By 54 GPa all sharp crystalline peaks disappeared from observed Raman spectra indicating complete pressure-induced amorphization (PIA). The amorphous $(Mg,Fe)_2SiO_4$ spectrum contains Si-O stretching bands at lower wavenumber than expected for SiO_4^{4-} indicating high coordination of the silicate units. The amorphous spectrum persisted on decompression to ambient conditions but with evidence for reappearance of tetrahedrally coordinated units. Non-hydrostatic compression of polycrystalline olivine samples showed similar appearance of the defect feature and broad amorphous features between 43–44 GPa. Both increased in intensity as the sample was left at pressure overnight but they disappeared during decompression below 17 GPa with recovery of the starting olivine Raman signature. A hydrated San Carlos olivine sample containing 75–150 ppm OH was also studied. Significant broadening of the SiO_4^{4-} stretching peaks was observed above 43 GPa but without immediate appearance of the defect or broad amorphous features. However, both of these characteristics emerged after leaving the sample at 47 GPa overnight followed by complete amorphization that occurred upon subsequent pressurization to 54 GPa. During decompression the high-density amorphous spectrum was retained to 3 GPa but on final pressure release a spectrum similar to thermally quenched low-pressure olivine glass containing isolated SiO_4^{4-} groups was obtained. Leaving this sample overnight resulted in recrystallization of olivine. Our experimental data provide new insights into the metastable structural transformations and relaxation behavior of olivine samples including material recovered from meteorites and laboratory shock experiments.

Keywords: San Carlos olivine, Raman spectroscopy, metastable phase transition, defect formation, amorphization, high-density silicate glass

Introduction

Olivine [α-$(Mg,Fe)_2SiO_4$] is the dominant mineral of the Earth's upper mantle and is present within chondritic meteorites as well as a wide range of other extra-terrestrial environments [see Finkelstein et al. (2014) for a summary of literature]. It is important to understand the stable and metastable structural transformations that occur for this important mineral phase as it experiences static and dynamic compression followed by recovery to ambient conditions. Equilibrium phase relations within the Mg_2SiO_4-Fe_2SiO_4 system are well established from high pressure–high temperature (*P*-*T*) experiments. α-Mg_2SiO_4 (forsterite; Fo) transforms first into spinelloid β-Mg_2SiO_4 (wadsleyite) and then spinel-structured γ-Mg_2SiO_4 (ringwoodite) phases at between P = 12–22 GPa depending upon the temperature, before chemically dissociating into $MgSiO_3$ perovskite (bridgmanite) + MgO above ~25 GPa. The α-Fe_2SiO_4 end-member (fayalite, Fa)

* E-mail: p.f.mcmillan@ucl.ac.uk

0003-004X/16/0007–1642$05.00/DOI: http://dx.doi.org/10.2138/am-2016-5389CCBY

transforms directly into its spinel-structured γ-phase at $P = 6–7$ GPa. Changes in density, elastic properties, and mineral rheology associated with the α-β-γ phase transitions in the Mg_2SiO_4-Fe_2SiO_4 system are used to interpret the seismic discontinuities observed within the Earth's upper mantle and transition zone (Ringwood 1991). High *P-T* transformations of Fo-Fa olivine solid solutions also give rise to the wadsleyite and ringwoodite phases found among chondritic meteorite samples.

Metastable structural transformations and phase changes are encountered as $(Mg,Fe)_2SiO_4$ olivine is pressurized beyond its normal stability limits at low temperature or on rapid timescales. Mao and Bell (1972) measured electrical conductivity and optical absorption spectra of fayalite up to 30 GPa and reported a large conductivity increase and a red shift in the optical absorption edge. Shulien et al. (1978) recorded a similar conductivity increase during shock experiments for natural Fe-rich dunite. Mashimo et al. (1980) subjected single crystals of synthetic fayalite to shock compression between 19.5–56 GPa and confirmed the large increase in electrical conductivity. They noted a change in Hugoniot slope at around 30 GPa suggesting the presence of a phase transformation. Williams et al. (1990) obtained X-ray diffraction, IR and visible absorption spectroscopy, and electrical conductivity data for Fe_2SiO_4 olivine in the diamond-anvil cell (DAC). The band gap closure and conductivity increase were interpreted as due to increased interactions and possible electronic disproportionation between the Fe^{2+} ions. Pressure-induced amorphization (PIA) was proposed to occur above 39 GPa associated with an increase in the average local coordination of silicate units. However, the coordination change was not retained during decompression to ambient conditions. X-ray diffraction results obtained by Richard and Richet (1990) in the DAC likewise indicated amorphization of metastably compressed fayalite at 35 GPa. They found that the amorphous phase could be recovered to room pressure, but that the silicate units reverted to fourfold coordination during decompression.

The occurrence of PIA among Mg-rich olivine samples is less well documented. Jeanloz et al. (1977) reported amorphous zones occurring within a natural $(Mg_{0.88}Fe_{0.12})_2SiO_4$ crystal shocked in the laboratory to >56 GPa. However, Jeanloz (1980) later examined single-crystal samples of $(Mg,Fe)_2SiO_4$ olivines recovered following shock compression to between 25–70 GPa using TEM and IR spectroscopy. He concluded that the amorphous zones observed previously corresponded to localized regions of intense strain that constituted no more than a few percent of any sample. Heymann and Cellucci (1988) examined a shocked sample of natural dunite using Raman spectroscopy and observed a broad feature at 1100 cm^{-1} that they interpreted as due to olivine glass formed during the shock experiment. However, during a later study of a suite of shocked chondrite samples, Heymann (1990) concluded that the feature was mainly due to luminescence effects. Guyot and Reynard (1992) subjected San Carlos olivine $(Mg,Fe)_2SiO_4$ samples to high *P-T* treatment at temperatures below 700 °C in a laser-heated DAC. They observed that samples recovered from >70 GPa appeared amorphous to examination by transmission electron microscopy (TEM) and electron diffraction, but materials recovered from lower pressure (30–70 GPa) showed the presence of intermediate crystalline phases with a hexagonally close packed (hcp) lattice. Andrault et al. (1995) carried out in situ energy-dispersive X-ray diffraction at up to 50–69 GPa for olivines along the Mg_2SiO_4-Fe_2SiO_4 join. They observed PIA occurring for fayalite as previously reported, but observed that although broad amorphous features were observed to occur at increasingly higher pressures as the Fo content increased, some crystalline diffraction remained for all the other samples to the highest pressures examined. They concluded that PIA occurred as a continuous transformation process within parts of the crystalline samples, and that the metastable transformations could be associated with a kinetically frustrated structural transition to wadsleyeite (β-Mg_2SiO_4) or another spinelloid type structure.

Raman spectroscopic investigations of $(Mg,Fe)_2SiO_4$ olivines recovered from natural meteorites as well as laboratory shocked samples have revealed additional peaks in the 600–800 cm^{-1} range that are not predicted to occur for the olivine structure (Farrell-Turner et al. 2005; Van de Moortèle et al. 2007). A similar band observed to appear in the Raman spectra of polycrystalline α-Mg_2SiO_4 compressed to above 31 GPa was assigned to the formation of local "defects" associated with Si-O-Si linkages involving highly coordinated SiO_n (e.g., n = 5,6) species (Durben et al. 1993). An analogous feature was also noted to appear for β-Mg_2SiO_4 samples heated metastably at ambient pressure (McMillan et al. 1991). Van de Moortèle et al. (2007) combined their Raman and TEM observations of unusual dark-colored veins of shocked olivine in two martian meteorites (NWA 2737 and NWA 1950) with MD simulation results to suggest possible formation of a metastable $(Mg,Fe)_2SiO_4$ phase from shock compression of Mg-rich olivine to between 35–50 GPa. However, the proposed ζ-$(Mg,Fe)_2SiO_4$ structure did not contain any highly coordinated silicate species.

Finkelstein et al. (2014) have carried out a detailed structural investigation of α-Mg_2SiO_4 using single-crystal X-ray diffraction during hydrostatic compression to 90 GPa. They observed that the forsterite structure remained intact up to 48 GPa and they identified phase transitions occurring within the metastably compressed material at 50 and 58 GPa to two new polymorphs labeled forsterite (Fo-) II and III, respectively. These structures and metastable phase transitions were identified by ab initio evolutionary crystal structure prediction and metadynamics simulations carried out using density functional theory (DFT). The new phases contain SiO_4 and SiO_6 units connected by Si-O-Si linkages formed between the previously isolated SiO_4^{4-} tetrahedra, and fivefold-coordinated SiO_5 species were also suggested to appear during the metastable structural transformation process from olivine.

In the present work we report Raman spectroscopic results for single-crystal and polycrystalline samples of natural San Carlos $(Mg,Fe)_2SiO_4$ olivine compressed under hydrostatic and non-hydrostatic conditions to 57 GPa. We also completed density functional theory (DFT) calculations on the Mg end-member olivine (Mg_2SiO_4, forsterite) using the CRYSTAL14 code (Dovesi et al. 2014) to help interpret the experimental data. Our compression results differ from those of Finkelstein et al. (2014) in that we observe appearance of "defect" features associated with formation of SiOSi linkages and highly coordinated SiO_5 or SiO_6 species above 42 GPa within the single-crystalline sample, along with PIA that is completed by 54 GPa. The amorphous solid is recovered to ambient conditions and it clearly contains

highly coordinated silicate species, and it is different from olivine glass produced by quenching from the melt phase. Slightly different compression and decompression behavior is observed for polycrystalline and OH-containing samples. We discuss these observations in terms of metastable transformations occurring for $(Mg,Fe)_2SiO_4$ olivine materials and highlight their importance for analyzing and interpreting materials recovered from meteorite samples as well as static and dynamic compression experiments.

Experimental methods

Our crystals were extracted from the same xenolith as the material studied by Demouchy and Mackwell (2006). Electron microprobe analyses gave the composition $(Mg_{1.81}Fe_{0.18}Ni_{0.01})_2SiO_4$ typical for San Carlos olivine (Fournelle 2011). The OH content was below the detection limit for Fourier transform infrared (FTIR) spectroscopy (<1 ppm H_2O). For our first series of room-temperature pressurization experiments a polished single-crystal of approximate dimensions 14 × 22 × 8 μm^3 was oriented with its b axis perpendicular to the diamond culet and placed in a 80 μm hole of a Re gasket pre-indented to 32 μm. Pressurization and decompression studies were carried out using a He gas membrane-drive diamond-anvil cell (DAC) (Almax-Easylab) with beveled diamond anvils (150 μm outer culet). Pressure was determined by ruby fluorescence. Helium was introduced into the cell by high-pressure gas loading to act as a hydrostatic pressure-transmitting medium (PTM) (Klotz et al. 2009).

A second series of experiments was designed to investigate the compression behavior of olivine under non-hydrostatic conditions. A polycrystalline material was produced by grinding the crystals in an agate mortar to produce micrometer-sized grains. The resulting powder was then pressed into a pellet and loaded into the cell using Ne as PTM. Although Ne solidifies at 4.8 GPa, it only leads to obvious signs of non-hydrostatic broadening in the ruby R1 fluorescence line above 15 GPa (Klotz et al. 2009). However, a range of highly non-hydrostatic pressurization conditions occurs throughout the polycrystalline pressed powder sample at all pressures as a result of intergrain contacts that provide high energy sites to initiate phase changes.

In a third experiment the effect of incorporated OH on the compression behavior of $(Mg,Fe)_2SiO_4$ olivine was investigated. OH-enriched olivine was prepared by treating San Carlos crystals ground to an initial grain size <50 μm at ~7 GPa and 1273 K in a multi-anvil device for 43 h. The olivine powder was packed into a graphite sleeve that was then arc-welded inside a Pt capsule. A 1.4:1 by weight talc:brucite mixture was loaded in one end of the Pt capsule. This dehydrated at run conditions to produce forsterite + enstatite + H_2O thus providing a source of H_2O as well as buffering a_{SiO_2} during the experiment. Pressure within the multi-anvil apparatus was estimated to within ±1 GPa. The recovered Pt capsule released free water upon piercing and the grain size of the initial San Carlos olivine had increased to several hundred micrometers, consistent with the sample being held under water saturated conditions during the high *P-T* experiment. Unpolarized FTIR spectra of recovered crystals indicated a water content between 75–150 ppm (Withers et al. 2012). This value is similar to H_2O contents observed for samples hydrated in the presence of H_2O-CO_2 fluids (Yang et al. 2014), but is lower than the maximum OH solubility in olivine at similar *P-T* conditions in equilibrium with pure H_2O (Kohlstedt et al. 1996). A fragment of the OH-saturated olivine crystal ~20 × 20 × 10 μm in dimensions was loaded into the DAC and compressed using He as PTM.

Raman spectra were measured in backscattering geometry with resolution <2 cm^{-1} using home-built and commercial instruments in London (UCL) and in Valencia at up to 58 GPa. The UCL instrument was built around an Acton 300 spectrometer and liquid N_2-cooled back-illuminated Si CCD detector (Princeton Instruments) using Kaiser holographic supernotch filters to discriminate between incident laser and Raman scattered light (Soignard and McMillan 2004). Spectra were obtained using 514.5 or 488 nm lines from an Ar^+ laser focused on the sample using a Mitutoyo 50× long working distance (LWD) objective. In Valencia spectra were obtained using: (1) a LabRAM HR UV microspectrometer coupled to a Peltier-cooled CCD detector. The 532 nm line of a solid state laser was focused on the sample using a 50× LWD objective and light was dispersed on to the detector with a 1200 gr/mm grating; (2) a home-built microscopic confocal system using 488 nm Ar^+ laser excitation and a Semrock edge filter to discriminate against elastically scattered light. The Raman signal was dispersed via a Jobin-Yvon TRH 1000 spectrometer (1200 gr/mm grating) on to a thermoelectric-cooled multichannel Synapse CCD detector. Wavenumbers of all Raman instruments and experiments were calibrated using laser plasma lines and a Ne lamp.

Density functional theory (DFT) calculations on the Mg end-member olivine (Mg_2SiO_4, forsterite) were performed using the CRYSTAL14 code (Dovesi et al. 2014) using the B3LYP hybrid exchange functional and the basis set from Noel et al. (2006). Structures of the forsterite-I, -II, and -III phases at different volumes were taken from Finkelstein et al. (2014), followed by constant volume geometry optimizations before calculation of their zone-center Raman spectra. The Fo-III phase at the 58.2 GPa volume yielded imaginary phonons in the $Cmc2_1$ space group reported by Finkelstein et al. (2014). The crystallographic unit cell (4 formula units) was reoptimized without symmetry, revealing small symmetry breaking atomic displacements that result in the structure remaining within the $P1$ space group. Raman intensities were calculated using the CPKS method discussed in Maschio et al. (2013a, 2013b). The data are presented as orientationally and polarization averaged powder spectra appropriate for the 180° backscattering geometry used experimentally (Prosandeev et al. 2005).

Molecular dynamics (MD) simulations were carried out to further investigate the vibrational properties of the metastably compressed phases. We used a similar protocol to that described in our previous study of another metastable phase ("ζ-Mg_2SiO_4") predicted to form from olivine during dynamic compression (Van de Moortèle et al. 2007). The calculations were carried out using an Anisotropic Ion Model (AIM) (Aguado et al. 2003), in which induced ion moments and short-range size and shape deformations of O^{2-} parametrized via high-level electronic structure calculations (Jahn and Madden 2007) were included to quadrupolar level. The simulation contained 672 ions under constant P conditions with variable volume and cell dimensions at T = 300 K. The vibrational densities of states (VDOS) for the compressed structures were calculated by extracting 10 configurations at each pressure with each time-separated by ~100 ps. The Hessian matrix with elements

$$H_{i\mu,j\nu} = \frac{1}{m}\frac{\partial^2 U}{\partial r_{i,\alpha}\,\partial r_{j,\beta}}$$

(U is the total system energy for a given configuration $\{\mathbf{R}^N\} = \{\mathbf{r}_1, \mathbf{r}_2, .., \mathbf{r}_N\}$) was calculated numerically and diagonalized to obtain the VDOS.

Results

Mg_2SiO_4 olivine has an orthorhombic unit cell, space group *Pbnm*, containing slightly distorted (SiO_4) tetrahedra along with two types of (MgO_6) octahedra (M1 and M2 sites) (Birle et al. 1968). With Z = 4 formula units in the primitive unit cell, symmetry analysis predicts 84 vibrational modes at the Brillouin zone center. Of these, 36 are Raman active: $\Gamma_{Raman} = 11\ A_g + 11\ B_{1g} + 7\ B_{2g} + 7\ B_{3g}$ that have been assigned to their respective atomic displacement patterns from polarized single-crystal studies and isotopic exchange experiments along with empirical force field, ionic model and ab initio density functional theory (DFT) calculations (Servoin and Piriou 1973; Pâques-Ledent and Tarte 1973; Iishi 1978; Price et al. 1987; Chopelas 1991; Kolesov and Geiger 2004; Noel et al. 2006). The principal Raman peaks are the Si-O stretching modes derived from coupled vibrations of the SiO_4^{4-} tetrahedra that occur between 800–1000 cm^{-1} at ambient pressure (Fig. 1). Studies of single-crystalline samples show changes in relative peak intensities as a function of orientation and polarization conditions (Servoin and Piriou 1973; Iishi 1978; Chopelas 1991; Kolesov and Geiger 2004). In our experiments we did not collect polarized data but instead oriented our sample to ensure that all major peaks were represented in the spectra. The pattern of relative peak intensities resembled the *cc* data of Kolesov and Geiger (2004) (A_g modes) for a $Fo_{90}Fa_{10}$ sample, with the addition of B_{3g} and B_{2g} peaks (Fig. 1). The use of a membrane-driven DAC that remained mounted in the beam while changing pressure allowed us to maintain the sample orientation throughout each series of experiments.

In addition to Raman scattering, olivine vibrational spectra have also been studied extensively by FTIR and inelastic neutron scattering (INS) spectroscopy, as well as by ion dynamics

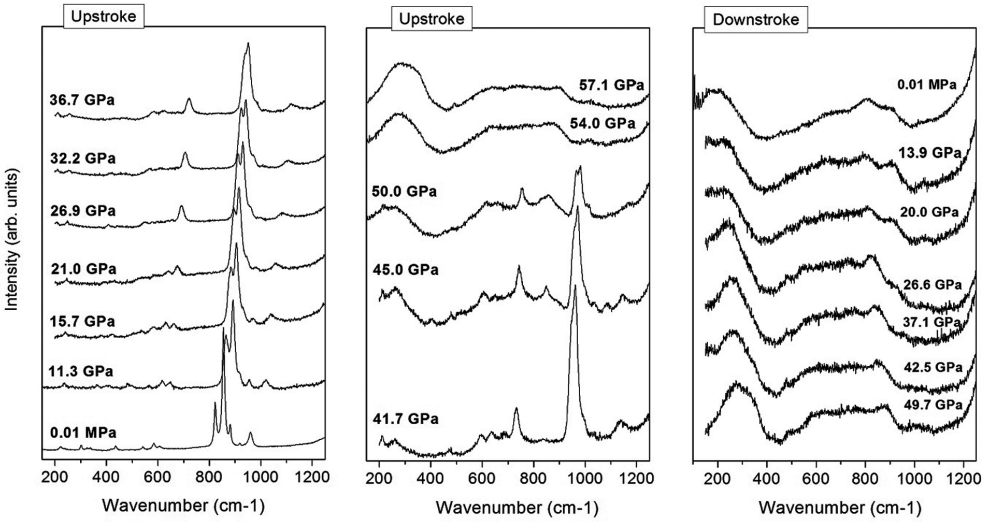

FIGURE 1. Room-temperature Raman scattering spectra of single-crystal San Carlos olivine during quasi-hydrostatic compression in He at selected pressures up to 57 GPa on the upstroke and during decompression to 1 atm.

simulations and first principles vibrational studies, to reveal the distribution of modes occurring throughout the Brillouin zone (Servoin and Piriou 1973; Hofmeister 1987, 1997; Rao et al. 1988; Price et al. 1987; Ghose et al. 1991; Noel et al. 2006). The modes observed are distributed according to the following groupings: ν_1 and ν_3 internal Si-O stretching of the SiO_4^{4-} tetrahedra in the 820–980 cm^{-1} range; SiO_4^{4-} ν_2 and ν_4 bending between 420–650 cm^{-1}, and librational modes involving Mg^{2+} cations and SiO_4 units below 470 cm^{-1}. Of particular importance for interpretation of our data is that no Raman peaks, or indeed any phonons propagating throughout the Brillouin zone, occur in the range 650–820 cm^{-1}, between the tetrahedral bending and stretching modes.

We obtained Raman spectra of our single-crystalline sample of San Carlos olivine compressed quasi-hydrostatically in He at up to 57.1 GPa (Fig. 1). The data exhibit slight peak broadening above 11 GPa leading to loss of definition among the high-frequency modes, and the A_g mode in the 600–680 cm^{-1} region that is derived from ν_2 deformation of the SiO_4 units, becomes more prominent above 15.7 GPa. Our DFT calculations for Mg_2SiO_4 olivine based on fully isotropic averages of the derived polarizability tensor elements (Noel et al. 2006) show a similar intensification of this peak (Fig. 2) so that the effect must be due to changes in vibrational coupling among modes of the same symmetry (Piriou and McMillan 1983). Both the observed and calculated peak frequencies ($d\nu_i/dP$) show a regular variation with pressure, in good agreement with previous studies (Chopelas 1990, 1991) (Fig. 3). The >200 cm^{-1} separation between the internal SiO_4^{4-} stretching and bending modes is maintained throughout the pressure range.

At 41.7 GPa, a new peak appears in the experimental data within the previously blank region between the SiO_4 stretching and bending vibrations. This peak first appears at 820 cm^{-1} and shifts to 840 cm^{-1} by 50 GPa (Fig. 1). A similar peak was noted to appear in the same pressure range In a previous Raman study of polycrystalline α-Mg_2SiO_4 compressed in Ar to 50 GPa (Durben et al. 1993). As already noted, no vibrational features are expected to occur in this intermediate range between the SiO_4 stretching and bending vibrations for the olivine structure (Rao et al. 1988; Price et al. 1987; Ghose et al. 1991; Noel et al. 2006) and none appear in our DFT calculations for the compressed Mg_2SiO_4 forsterite phase (Fig. 2). Durben et al. (1993) proposed that the new peak might indicate the formation of SiOSi linkages between adjacent SiO_4^{4-} tetrahedra resulting in the appearance of highly coordinated species (e.g., SiO_5 or SiO_6 units) that could be present as localized defects within the structure. Examination of the atomic displacement patterns for the vibrational modes of the Fo-II and Fo-III structures allow us to refine that interpretation. In Fo-II we have both SiO_4 and SiO_6 units connected by an SiOSi linkage. The peak at 895 cm^{-1} corresponds to a Si-O

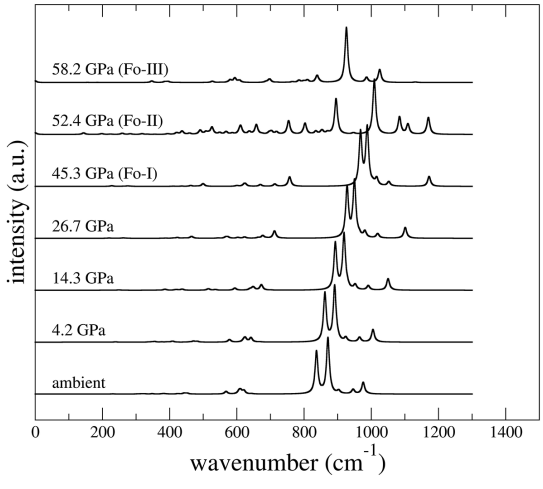

FIGURE 2. Raman spectra of Mg_2SiO_4 olivine calculated using first-principles DFT methods up to 45.3 GPa along with DFT calculations of spectra for Fo-II and Fo-III phases identified by Finkelstein et al. (2014) at 52.4 and 58.2 GPa, respectively.

stretching vibration of the octahedral units concentrated on the non-bridging O atoms bonded to Mg^{2+} cations. The SiOSi stretching vibration of the oxygen linking the SiO_4 and SiO_6 groups appears at 1083 cm^{-1}, whereas the remaining high-frequency modes at 1009, 1108, and 1169 cm^{-1} are mainly SiO_4 stretching vibrations involving the non-bridging O atoms. In Fo-III, all Si atoms are sixfold-coordinated, but there is one very short Si-O bond (1.64 Å), one medium (1.70 Å), and four long (1.77 Å). The main peaks are: 926 cm^{-1}: stretching of the long Si-O bond, connected to 4 Mg^{2+} cations; 1025 cm^{-1}: stretching of the short Si-O bond, connected to 3 Mg^{2+} cations; 986 cm^{-1}: stretching of the SiOSi linkage between adjacent SiO_6 units. During our discussion, we continue to refer to the new peak that appears in the olivine spectrum in the 800–900 cm^{-1} region as a "defect" feature, associated with the presence of highly coordinated SiO_6 or SiO_5 species, formed by creating SiOSi linkages with adjacent SiO_4^{4-} units.

At the same pressure, broad background features also begin to appear underlying the sharp crystalline peaks that are maintained in the spectra up to between 50–54 GPa (Fig. 1). Above 54 GPa, the spectrum consists entirely of these broad features that are typically interpreted as indicative of amorphous material. These are maintained during decompression to ambient conditions (Fig. 1). The Raman spectrum of the recovered sample differs substantially from that of olivine glass prepared by quenching from the melt at ambient pressure that is dominated by a strong band near 850 cm^{-1} due to the ν_1 symmetric stretching of isolated SiO_4^{4-} units (Piriou and McMillan 1983; Williams et al. 1989).

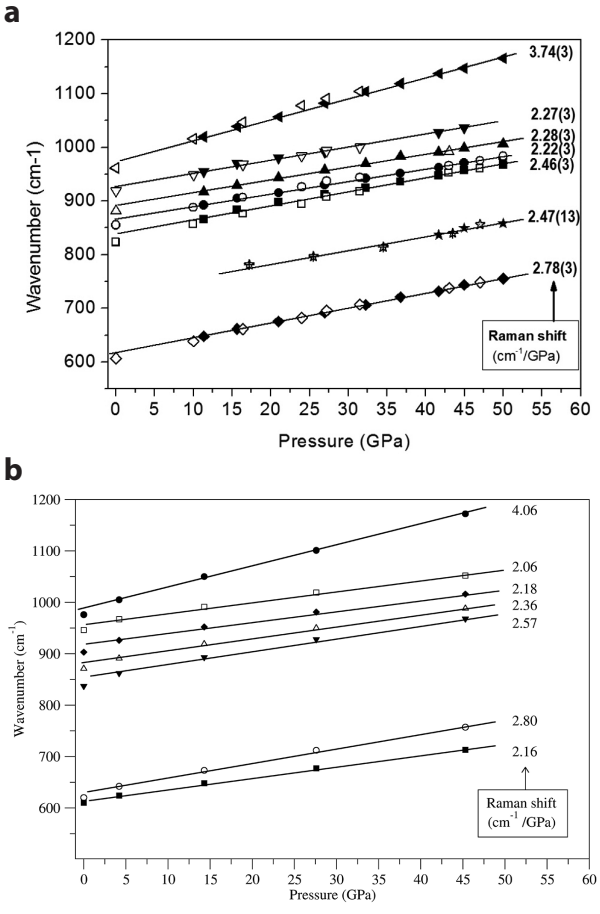

FIGURE 3. Pressure dependence of Raman active modes above 600 cm^{-1} for olivine samples. (**a**) The experimental data for San Carlos $(Mg,Fe)_2SiO_4$ olivines include natural (solid symbols) and OH-enriched (empty symbols) samples. The ν_2 SiO_4 bending vibration that shows an intensity increase above 31 GPa for all samples is seen to maintain the same dν/dP relation throughout the compression experiments. The new "defect" Raman mode that appears above 40 GPa during compression of olivine samples is shown as starred symbols. Crossed stars correspond to the peak retained to lower pressure during decompression for powdered San Carlos olivine. The (dν/dP) relation can be extrapolated to a frequency near 730 cm^{-1} at ambient pressure, corresponding to features observed for naturally and laboratory-shocked olivine samples. (**b**) Pressure dependence of Raman active modes for Mg_2SiO_4 forsterite calculated using first-principles DFT techniques.

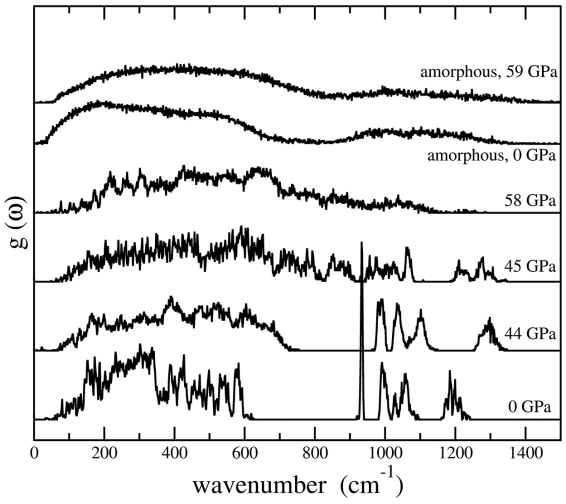

FIGURE 4. Anisotropic ion molecular dynamics (AIMD) simulations of the vibrational density of states [VDOS, g(ω)] of Fo-I (a-Mg_2SiO_4) at 0 and 44 GPa, Fo-II at 45 GPa and Fo-III at 58 GPa, compared with simulated VDOS spectra of amorphous Mg_2SiO_4 quenched from the simulated liquid state at 0 and 59 GPa.

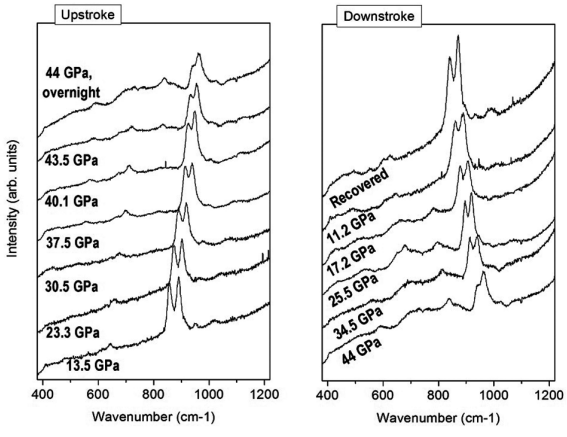

FIGURE 5. Room-temperature Raman scattering spectra of San Carlos olivine powder at selected pressures up to 44 GPa.

Instead, the amorphous solid produced by PIA shows a broad band of vibrational excitations at lower wavenumbers indicating the presence of highly coordinated silicate species. The Raman spectrum of the high-density amorphous solid evolved slightly during decompression with development of intensity in the 850–900 cm^{-1} range below 27 GPa, indicating the re-appearance of some proportion of tetrahedral SiO_4 units within the structure. The vibrational density of states (VDOS) functions of simulated amorphous Mg_2SiO_4 prepared by quenching from the liquid state in AIMD calculations at 0 and 59 GPa are compared in Figure 4.

We continued with an investigation of powdered $(Mg_{0.88}Fe_{0.12})_2SiO_4$ olivine compressed using Ne as a PTM to study the metastable transformation behavior under highly non-hydrostatic conditions (Fig. 5). The Raman peaks exhibited additional broadening by 13.5 GPa due to deviatoric stresses generated within the pressed powdered sample. However, as observed for the single-crystal sample, a new 830 cm^{-1} "defect" peak appeared by ~43.5 GPa. After allowing the sample to relax overnight, this peak increased in intensity, and a broad amorphous background emerged underlying the crystalline features. The sample was not pressurized further so that the crystalline peaks did not disappear. During decompression the characteristic Raman peaks of crystalline olivine re-emerged immediately, although the defect feature was still observed down to 17 GPa. The position of this peak extrapolated to ambient pressure indicated a value near 720 cm^{-1} (Fig. 3), close to that of the additional defect feature noted previously in spectra of natural and laboratory shocked olivine samples (Heymann 1990; Heymann and Cellucci 1988; Farrell-Turner et al. 2005; Van de Moortèle et al. 2007). Following complete recovery to ambient conditions, the main features of the crystalline olivine spectrum reappeared but with different relative intensities of the two main Si-O stretching peaks, and the remaining bands were broadened compared with the starting material (Fig. 5).

We completed our study by compression and decompression of a hydrated sample prepared from San Carlos olivine to investigate the effects of dissolved OH on the metastable transformations and their kinetics (Fig. 6). Upon raising the pressure between 31.5 and 47 GPa, the overall intensity of the Raman spectrum decreased markedly, and the Si-O tetrahedral stretching features became broadened and less well resolved. The sample was then left overnight at 47 GPa. A further reduction in overall Raman intensity was noted and broad amorphous features along with the "defect" peak near 880 cm^{-1} appeared in the spectrum. Further compression to 50–54 GPa led to further broadening and disappearance of the highest frequency Si-O stretching band in the 1000–1100 cm^{-1} region. The Raman spectrum of this apparently amorphous OH-containing olivine sample was retained during decompression, with re-appearance of broadened crystalline peaks below 3 GPa. The high-frequency feature resembled the tetrahedral SiO_4^{4-} stretching of olivine glass produced by melt quenching (Piriou and McMillan 1983; Williams et al. 1989). The appearance of this feature was detected in the Raman spectrum taken at 8 GPa (Fig. 6). Following recovery to ambient conditions and leaving at 1 atm overnight, the crystalline olivine spectrum re-emerged. It is obvious that the presence of OH groups within the olivine structure affects both the nature and the kinetics of the metastable structural transformations, apparently favoring the retention and recovery of tetrahedrally bonded species.

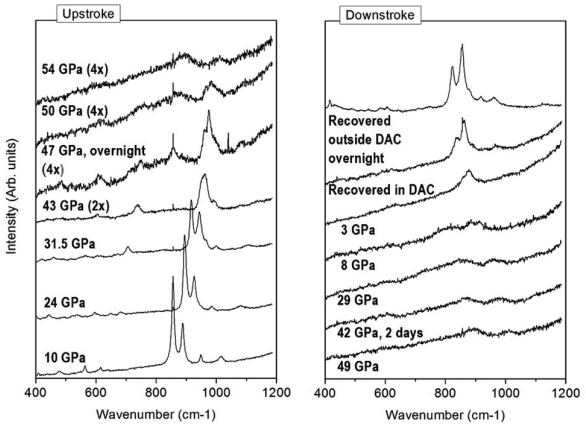

FIGURE 6. Room-temperature Raman scattering spectra of single-crystal OH-enriched San Carlos olivine powder at selected pressures up to 54 GPa.

DISCUSSION

Our results obtained during hydrostatic compression of a single-crystalline San Carlos olivine sample composition suggest that localized defect structures associated with formation of SiOSi linkages between previously independent SiO_4^{4-} tetrahedra and associated with formation of five- or sixfold-coordinated silicate species occur within the structure above 41–42 GPa. Observation of the characteristic "defect" peak in the 800–900 cm^{-1} region that is normally free from vibrational modes for olivine structures coincides with the appearance of broad background features indicative of amorphous material. An initial conclusion would be that PIA has occurred with its onset near 41 GPa and completed by 54 GPa, initiated or accompanied by the formation of localized defects within the olivine structure.

Both our results and this interpretation differ from those of Finkelstein et al. (2014), who studied end-member single-crystalline Mg_2SiO_4 compressed hydrostatically in He under similar conditions to our experiment, using single-crystal X-ray structural refinement to follow structural changes in the material. Combining the X-ray results with ab initio structure searching and metadynamics simulations they identified metastable crystalline phase transitions occurring at 50 and 58 GPa into two new phases (Fo-II and Fo-III). They observed that the initial olivine structure (Fo-I) was maintained metastably up to 48 GPa, with no indication of local defect formation or amorphization. Above this pressure an abrupt transition occurred into the Fo-II phase at 50 GPa, quickly followed by a second transition into the Fo-III phase upon further compression to 58 GPa. The ab initio searching and metadynamics calculations confirmed the structures that were shown to contain interconnected SiO_4 and SiO_6 units, while intermediate SiO_5 species were also identified during the metastable structural transformation process from olivine (Finkelstein et al. 2014).

Those observations lead to a possible alternative interpretation of our results. Our DFT calculations of the Raman spectra of Fo-II using the structural parameters provided by Finkelstein et al. (2014) at 52.4 GPa show they are dominated by strong peaks

at 890 and 990 cm^{-1} at this pressure (Fig. 2). It might be possible that the broadening and loss of resolution we observe in the high-frequency SiO_4^{4-} stretching peaks along with the appearance of the "defect" feature at 41.7 GPa could be associated with formation of domains of the Fo-II structure within the natural single sample, at a lower pressure than that found by Finkelstein et al. (2014), perhaps due to the presence of Fe^{2+} ions within the San Carlos olivine. The simultaneous appearance of broad background scattering could either be due to macroscopically amorphous domains produced within the sample due to the kinetically hindered phase transformation and localized defects produced within the olivine structure, or could indicate a mixture of the vibrational density of states (VDOS) from both Fo-I and Fo-II activated at the Brillouin zone center by the presence of local defects and structural intergrowths that impede the propagation of lattice vibrations. Our AIMD simulations demonstrate that the VDOS for metastably compressed Fo-I exhibits the expected gap between SiO_4^{4-} deformation and tetrahedral stretching modes between 750–980 cm^{-1} at 44 GPa, whereas the Fo-II vibrations extend throughout this region and up to 1320 cm^{-1} at around the same pressure (45 GPa) (Fig. 4). Our observation of the initial olivine "internal defect" formation coupled with the onset of PIA could in fact reflect the occurrence of the metastable Fo-I to Fo-II phase transformation at significantly lower pressure (41 vs. 50 GPa) in the Fe^{2+}-containing natural sample.

In our study we observed complete amorphization occurring by 54 GPa for the olivine single crystal, with broad amorphous Raman bands observed between 200–400 cm^{-1} and extending throughout the 500–900 cm^{-1} region (Fig. 1). The Raman spectrum calculated by DFT for the Fo-III structure at 58.2 GPa shows a single strong peak at 930 cm^{-1} (Fig. 2). However, the VDOS obtained from AIMD simulations of this phase shows a featureless broad band extending between 100–1100 cm^{-1} at the same pressure (59 GPa), with perhaps a more prominent feature developed near 670 cm^{-1} (Fig. 4). The VDOS for the high-pressure crystal differs from the simulated spectrum of a high-density Mg_2SiO_4 glass quenched from the liquid state at 59 GPa. Here there is an enhanced contribution from the higher frequency Si-O stretching vibrations at higher wavenumber values due to the presence of four- and fivefold-coordinated silicate species. The average Si^{4+} coordination by O^{2-} ions is 5.14 compared with 3.96 for an Mg_2SiO_4 melt quenched at P = 0 GPa (Fig. 4). The low-pressure quenched liquid exhibits an enhanced intensity in the 900–1300 cm^{-1} region, with a clear separation from the lower frequency SiO_4^{4-} deformation modes, and prominent feature at 150–200 cm^{-1} due to Mg-O vibrations and SiO_4^{4-} librations.

During low-temperature compression of crystalline samples into a highly metastable densified regime, there is always a delicate balance between kinetic and thermodynamic factors determining structural changes and phase transformations occurring in metastable phase space. In addition, the use of different methods to observe and diagnose metastable crystalline transitions vs. PIA can lead to different interpretations depending on the characteristic length scale of the probe techniques used (Machon et al. 2014). Because the structural transformations are kinetically hindered they can result in non-equilibrium pathways and materials produced both at high pressure and recovered to ambient conditions. In the case of PIA investigations, the use of single crystals vs. powdered samples, or the presence of compositional impurities, as well as the nature and rate of compression conditions can substantially affect the results and their interpretations (Kingma et al. 1993; Ekbundit et al. 1996; Machon et al. 2014). In addition, it is not always easy to determine from results such as X-ray diffraction or Raman scattering if defect formation or PIA has occurred, or if the data reveal kinetically hindered one or more metastable phase transitions involving potentially locally disordered phases. These considerations are clearly revealed here by comparison of our results with those of Finkelstein et al. (2014).

The thermodynamic possibilities for these different cases occurring can be interpreted by considering the free energy relations of metastably compressed phases (Machon et al. 2014). Any crystal subject to a first-order transformation into a high-density phase can be metastably compressed beyond its thermodynamic transition pressure if the temperature is too low or the compression rate too rapid to initiate and complete the expected phase change. However, no system can be compressed indefinitely without undergoing a fundamental mechanical, electronic, or phonon instability resulting in structural collapse. If this collapse occurs at too low temperature or on a too rapid timescale, ionic or atomic diffusion or bond rearrangements cannot take place to result in a new crystalline lattice and the result is as an amorphous solid. Alternatively, the metastably compressed crystal can undergo metastable phase transformations into new structural types as their free energy [$G(P)$] relations are intersected. Another event that can occur especially under non-hydrostatic pressurization conditions is that the material leaves the metastable extension of its free energy $G(P)$ curve at lower pressure but with insufficient thermal energy to achieve the formation of metastable crystals, to result in a solid amorphous material. Such a PIA process could have occurred during our metastable compression of $Fo_{90}Fa_{10}$ olivine under hydrostatic conditions above 41 GPa, where the presence of Fe^{2+} substituting for Mg^{2+} ions might have lowered local energetic barriers and thus affected the structural transformation kinetics.

The Raman signature of the dense amorphous solid produced by PIA and recovered following decompression from single-crystalline olivine following quasi-hydrostatic pressurization is notably different from that of thermal $(Mg,Fe)_2SiO_4$ glasses formed by quenching from the liquid state (Piriou and McMillan 1983; Williams et al. 1989). These glasses are dominated by a strong polarized peak near 850 cm^{-1} assigned to isolated SiO_4^{4-} stretching vibrations that is absent here. The Raman spectrum observed following PIA at high pressure clearly indicates a lower maximum in wavenumber values than the compressed orthosilicate crystal, demonstrating the presence of higher coordinated (SiO_5 or SiO_6) units in the amorphous state. However, the distribution of Raman peaks are also similar to the VDOS observed for the Fo-III crystalline material. The amorphous spectrum evolved during decompression indicated the reappearance of tetrahedrally bonded silicate units.

The formation of SiOSi linkages between adjacent SiO_4 tetrahedral units that results in the appearance of SiO_5/SiO_6 species within metastably compressed olivine might represent an early stage in the crystalline disordering leading to global PIA or to

formation of Fo-II and Fo-III crystalline phases, occurring within the 40–45 GPa range at low temperature. Our studies also show that the defect formation and PIA processes continue to progress if the sample is held at 43–45 GPa on laboratory timescales. In the case of our powdered samples compressed non-hydrostatically to within this range an olivine phase is recovered but with evidence for nanoscale structural reorganization and disordering within the crystalline domains, and the defect Raman signature is retained down to low pressure (<17 GPa). During shock compression the amorphization and decompression timescales are much shorter and this might result in the defect feature that has been recorded in Raman spectra observed for naturally and laboratory shocked olivine samples (Farrell-Turner et al. 2005; Van de Moortèle et al. 2007).

Metastable compression of the OH-enriched olivine results in slightly different behavior indicating the effects of incorporated OH groups on the kinetics of metastable local structure changes and crystalline transformations. As for the "dry" samples, the SiOSi/SiO_5 defect feature is observed to appear above 42–43 GPa along with first evidence for broad amorphous Raman scattering. However, unlike materials with low-OH content, the amorphous phase produced by 50 GPa still retains Si-O stretching vibrations that are diagnostic of isolated SiO_4^{4-} species, presumably because of the presence of SiO_3(OH) groups that hinder oligomerization of adjacent silicate tetrahedra. However, by compression to 54 GPa, even these had mostly disappeared. During decompression, the high-pressure amorphous spectrum was maintained to below 29 GPa but a new feature indicated the re-emergence of SiO_4^{4-} units within structural environments similar to olivine in the 800–900 cm^{-1} region. As the pressure was reduced to 3 GPa the spectrum evolved to resemble that of olivine glass produced by quenching from the liquid phase (Piriou and McMillan 1983; Williams et al. 1989), followed by re-appearance of crystalline olivine peaks as the sample was recovered to ambient pressure conditions. The presence of OH groups within the olivine structure thus affects the structural transformation kinetics and pathways, especially during decompression. Previous studies have documented the effect of incorporated OH units in reducing the viscosity of olivine and this is typically attributed to an enhancement of Si^{4+} diffusion within the crystal (Karato et al. 1986; Mei and Kohlstedt 2000a, 2000b). However, one recent investigation found no evidence for enhanced Si diffusion in the presence of OH-bearing Mg_2SiO_4 forsterite, and even questioned the idea of significant hydrolytic weakening in olivine (Fei et al. 2013). Our results demonstrate that the presence of minor amounts of OH do affect the kinetics and transformation pathways of metastable structural and phase transitions in minerals at low temperatures where enhanced ionic diffusion is unlikely to be implicated.

Implications

Our results have implications for the interpretation of natural and synthetic olivine materials recovered following static and shock compression. Our diamond-anvil cell Raman results show that local defects and amorphous structures can appear within olivine crystals subjected to hydrostatic and non-hydrostatic compression at pressures lower than phase transitions found by single-crystal and ab initio compression experiments that set an upper limit for metastable crystal transformations under nearly equilibrium conditions. Laboratory shock and natural impact events occurring at low temperatures may result in defect structures and dense diaplectic glass retained within the olivine materials recovered and observed at ambient pressure. The diaplectic glass formed during shock events at low temperature is likely to be based on highly coordinated silicate species, but these will revert to tetrahedrally bonded orthosilicate glass structures if the glasses contain sufficiently high-OH content. Recrystallization is also expected to occur when polycrystalline materials are recovered following compression to pressures above 40 GPa, and the "defect" peak indicating local formation of SiOSi linkages and SiO_5 species may be lost. However, localally non-isotropic strain fields developed and maintained within crystalline grains in shocked meterorites can result in retention of such defect features in natural materials (Van de Moortèle et al. 2007). Our data place new constraints on the interpretation of natural and laboratory shocked olivine samples in terms of the *P-T* conditions that they have been exposed to.

Acknowledgments

Our work was supported by the U.K. NERC via Grant NE/K002902/1 and Spanish MINECO under projects MAT2014-46649-C4-1/2-P.

References cited

Aguado, A., Bernasconi, L., Jahn, S., and Madden, P.A. (2003) Multipoles and interaction potentials in ionic materials from planewave-DFT calculations. Faraday Discussions, 124, 171–184.

Andrault, D., Bouhifd, M.A., Itie, J.P., and Richet, P. (1995) Compression and amorphization of $(Mg,Fe)_2SiO_4$ olivines: An X-ray diffraction study up to 70 GPa. Physics and Chemistry of Minerals, 22, 99–107.

Birle, J.D., Gibbs, G.V., Moore, P.B., and Smith, J.V. (1968) Crystal structures of natural olivines. American Mineralogist, 53, 807–824.

Chopelas, A. (1990) Thermal properties of forsterite at mantle pressures derived from vibrational spectroscopy. Physics and Chemistry of Minerals, 17, 149–156.

——— (1991) Single-crystal Raman spectra of forsterite, fayalite and monticellite. American Mineralogist, 76, 1101–1109.

Demouchy, S., and Mackwell, S. (2006) Mechanisms of hydrogen incorporation and diffusion in iron-bearing olivine. Physics and Chemistry of Minerals, 33, 347–355.

Dovesi, R., Saunders, V.R., Roetti, C., Orlando, R., Zicovich-Wilson, C.M., Pascale, F., Civalleri, B., Doll, K., Harrison, N.M., Bush, I.J., and others. (2014) CRYSTAL14 User's Manual. University of Torino, Italy.

Durben, D.J., McMillan, P., and Wolf, G.H. (1993) Raman study of the high-pressure behavior of forsterite Mg_2SiO_4 crystal and glass. American Mineralogist, 78, 1143–1148.

Ekbundit, S., Leinenweber, K., Yarger, J.L., Robinson, J.S., Verhelst-Voorhees, M., and Wolf, G.H. (1996) New high-pressure phase and pressure-induced amorphization of $Ca(OH)_2$: Grain size effect. Journal of Solid State Chemistry, 126, 300–307.

Farrell-Turner, S., Reimold, W.U., Nieuwoudt, M., and Erasmus, R.M. (2005) Raman spectroscopy of olivine in dunite experimentally shocked to pressures between 5 and 59 GPa. Meteoritics and Planetary Science, 40, 1311–1327.

Fei, H., Wiedenbeck, M., Yamazaki, D., and Katsura, T. (2013) Small effect of water on upper-mantle rheology based on silicon self-diffusion coefficients. Nature, 498, 213–215.

Finkelstein, G.J., Dera, P.K., Jahn, S., Oganov, A.R., Holl, C.M., Meng, Y., and Duffy, T.S. (2014) Phase transitions and equation of state of forsterite to 90 GPa from single-crystal X-ray diffraction and molecular modelling. American Mineralogist, 99, 35–43.

Fournelle, J.H. (2011) An investigation of "San Carlos Olivine": comparing USNM-distributed material with commercially available material. Microscopy and Microanalysis, 17 (Supplement 2), 842–843.

Ghose, S., Hastings, J.M., Choudhury, N., Chaplot, S.L., and Rao, K.R. (1991) Phonon dispersion relation in faylaite, Fe_2SiO_4. Physica (B), 174, 83–86.

Guyot, F., and Reynard, B. (1992) Pressure-induced structural modifications and amorphization in olivine compounds. Chemical Geology, 96, 411–420.

Heymann, D. (1990) Raman study of olivines in 37 heavily and moderately shocked chondrites. Geochimica et Cosmochimica Acta, 54, 2507–2510.

Heymann, D., and Cellucci, T.A. (1988) Raman spectra of shocked minerals 1:

Olivine. Meteoritics, 23, 353–357.
Hofmeister, A.M. (1987) Single-crystal absorption and reflection spectroscopy of forsterite and fayalite. Physics and Chemistry of Minerals, 14, 499–513.
——— (1997) Infrared reflectance spectra of fayalite, and absorption data from assorted olivines, including pressure and isotope effects. Physics and Chemistry of Minerals, 24, 535–546.
Iishi, K. (1978) Lattice dynamics of forsterite. American Mineralogist, 63, 1198–1208.
Jahn, S., and Madden, P.A. (2007) Modelling Earth materials from crustal to lower mantle conditions: A transferable set of interaction potentials for the CMAS system. Physics of the Earth and Planetary Interiors, 162, 129–139.
Jeanloz, R. (1980) Shock effects in olivine and the implications for Hugoniot data. Journal of Geophysical Research, 85, 3163–3176.
Jeanloz, R., Ahrens, T.J., Lally, J.S., Nord, G.L. Jr., Christie, J.M., and Heuer, A.H. (1977) Shock-produced olivine glass: First observation. Science, 197, 457–459.
Karato, S.I., Paterson, M.S., and Fitz Gerald, J.D. (1986) Rheology of synthetic olivine aggregates—Influence of grain-size and water. Journal of Geophysical Research, 91, 8151–8176.
Kingma, K.J., Hemley, R.J., Mao, H.-k., and Veblen, D.R. (1993) New high-pressure transformation in α-quartz. Physical Review Letters, 70, 3927–3930.
Klotz, S., Chervin, J.-C., Munsch, P., and Le Marchand, G. (2009) Hydrostatic limits of 11 pressure transmitting media. Journal of Physics D: Applied Physics, 42, 075413.
Kohlstedt, D.L., Keppler, H., and Rubie, D.C. (1996) Solubility of water in the α, β and γ phases of $(Mg,Fe)_2SiO_4$. Contributions to Mineralogy and Petrology, 123, 345–357.
Kolesov, B., and Geiger, C. (2004) A Raman spectroscopic study of Fe-Mg olivines. Physics and Chemistry of Minerals, 31, 142–154.
Machon, D., Meersman, F., Wilding, M.C., Wilson, M., and McMillan, P.F. (2014) Pressure-induced amorphization and polyamorphism: Inorganic and biochemical systems. Progress in Materials Science, 61, 216–282.
Mao, H.K., and Bell, P.M. (1972) Electrical conductivity and red shift of absorption in olivine and spinel at high pressure. Science, 176, 403–406.
Maschio, L., Kirtman, B., Rérat, M., Orlando, R., and Dovesi, R. (2013a) *Ab initio* analytical Raman intensities for periodic systems through a coupled perturbed Hartree-Fock/Kohn-Sham method in an atomic orbital basis. I. Theory. Journal of Chemical Physics, 139, 164101.
——— (2013b) *Ab initio* analytical Raman intensities for periodic systems through a coupled perturbed Hartree-Fock/Kohn-Sham method in an atomic orbital basis. II. Validation and comparison with experiments. Journal of Chemical Physics, 139, 164102.
Mashimo, T., Kondo, K.I., Sawaoka, A., Syono, Y., Takei, H., and Ahrens, T.J. (1980) Electrical conductivity measurement of fayalite under shock compression up to 56 GPa. Journal of Geophysical Research, 85, 1876–1881.
Mason, B. (1963) Olivine composition in chondrites. Geochimica et Cosmochimica Acta, 27, 1011–1023.
McMillan, P.F., Akaogi, M., Sato, R.K., Poe, B., and Foley, J. (1991) Hydroxyl groups in β-Mg_2SiO_4. American Mineralogist, 76, 354–360.
Mei, S., and Kohlstedt, D.L. (2000a) Influence of water on plastic deformation of olivine aggregates 1. Diffusion creep regime. Journal of Geophysical Research, 105, 21457–21469.
——— (2000b) Influence of water on plastic deformation of olivine aggregates 2. Dislocation creep regime. Journal of Geophysical Research, 105, 21,471–21,481.
Noel, Y., Catti, M., D'Arco, Ph., and Dovesi, R. (2006) The vibrational frequencies of forsterite Mg_2SiO_4: An all-electron ab initio study with the CRYSTAL code. Physics and Chemistry of Minerals, 33, 383–393.
Pâques-Ledent, M.Th., and Tarte, P. (1973) Vibrational studies of olivine-type compounds-I. The IR and Raman spectra of the isotopic species of Mg_2SiO_4. Spectrochimica Acta, 29A, 1007–1016.
Piriou, B., and McMillan, P. (1983) The high-frequency vibrational spectra of vitreous and crystalline orthosilicates. American Mineralogist, 68, 426–443.
Price, G.D., Parker, S.C., and Leslie, M. (1987) The lattice dynamics of forsterite. Mineralogical Magazine, 51, 157–170.
Prosandeev, S.A., Waghmare, U., Levin, I., and Msalar, J. (2005) First-order Raman spectra of $AB'_{1/2}B''_{1/2}O_3$ double perovskites. Physical Review B, 71, 214307.
Rao, K.R., Chaplot, S.L., Choudhury, N., Ghose, S., Hastings, J.M., Corliss, L.M., and Price, D.L. (1988) Lattice dynamics and inelastic neutron scattering from forsterite, Mg_2SiO_4: Phonon dispersion relation, density of states and specific heat. Physics and Chemistry of Minerals, 16, 83–97.
Richard, G., and Richet, P. (1990) Room-temperature amorphization of faylaite and high-pressure properties of Fe_2SiO_4 liquid. Geophysical Research Letters, 17, 2093–2096.
Ringwood, A.E. (1991) Phase transformations and their bearing on the constitution and dynamics of the mantle. Geochimica et Cosmochimica Acta, 55, 2083–2110.
Schulien, S., Hornemann, U., and Stöffler, D. (1978) Electrical conductivity of dunite during shock compression from 12.5 to 45 GPa. Geophysical Research Letters, 5, 345–348.
Servoin, J.L., and Piriou, B. (1973) Infrared reflectivity and Raman scattering of Mg_2SiO_4 single crystal. Physica Status Solidi b, 55, 677–686.
Soignard, E., and McMillan, P.F. (2004) Defect chemistry in γ-Si_3N_4 and γ-Ge_3N_4 spinel nitride phases probed by Raman scattering in the laser-heated diamond anvil cell. Chemistry of Materials, 16, 3533–3542.
Van de Moortèle, B., Reynard, B., McMillan, P.F., Wilson, M., Beck, P., Gillet, P., and Jahn, S. (2007) Shock-induced transformation of olivine to a new metastable $(Mg,Fe)_2SiO_4$ polymorph in Martian meteorites. Earth and Planetary Science Letters, 261, 469–475.
Williams, Q., McMillan, P., and Cooney, T.F. (1989) Vibrational spectra of olivine composition glasses: The Mg-Mn join. Physics and Chemistry of Minerals, 16, 352–359.
Williams, Q., Knittle, E., Reichlin, R., Martin, S., and Jeanloz, R. (1990) Structural and electronic properties of Fe_2SiO_4-fayalite at ultrahigh pressures: Amorphization and gap closure. Journal of Geophysical Research, 95, 21,549–21,563.
Withers, A.C., Bureau, H., Raepsaet, C., and Hirschmann, M.M. (2012) Calibration of infrared spectroscopy by elastic recoil detection analysis of H in synthetic olivine. Chemical Geology, 334, 92–98.
Yang, X., Liu, D., and Xia, Q. (2014) CO_2-induced small water solubility in olivine and implications for properties of the shallow mantle. Earth and Planetary Science Letters, 403, 37–47.

Manuscript received April 28, 2015
Manuscript accepted January 22, 2016
Manuscript handled by Keith Putirka